

Nonlinear Processing with Linear Optics

Mustafa Yildirim^{1,2†}, Niyazi Ulas Dinc^{1,2†}, Ilker Oguz^{1,2}, Demetri Psaltis² and Christophe Moser¹

¹Laboratory of Applied Photonics Devices, Ecole Polytechnique Fédérale de Lausanne (EPFL), Switzerland

²Optics Laboratory, Ecole Polytechnique Fédérale de Lausanne (EPFL), Switzerland

† Equally contributing authors

Abstract

Deep neural networks have achieved remarkable breakthroughs by leveraging multiple layers of data processing to extract hidden representations, albeit at the cost of large electronic computing power. To enhance energy efficiency and speed, the optical implementation of neural networks aims to harness the advantages of optical bandwidth and the energy efficiency of optical interconnections. In the absence of low-power optical nonlinearities, the challenge in the implementation of multilayer optical networks lies in realizing multiple optical layers without resorting to electronic components. In this study, we present a novel framework that uses multiple scattering that is capable of synthesizing programmable linear and nonlinear transformations concurrently at low optical power by leveraging the nonlinear relationship between the scattering potential, represented by data, and the scattered field. Theoretical and experimental investigations show that repeating the data by multiple scattering enables non-linear optical computing at low power continuous wave light.

Optical computing has reemerged as an alternative to electronics for performing computations and handling information, particularly in the context of artificial intelligence applications. Optical neural networks (ONNs) hold promise in terms of speed and energy efficiency compared to traditional electronic computing¹. However, the development of fully optical ONNs has proven to be a challenging task due to the need for incorporating both linear and nonlinear computations within the optical domain². While several approaches have demonstrated efficient optical computing hardware for linear calculations³⁻⁷, effectively integrating these capabilities with nonlinear computations remains a significant obstacle for a complete realization of ONNs. Researchers have explored nonlinear light-matter interactions in the context of reservoir computing^{8,9}, employing high intensity pulsed lasers for nonlinear data processing¹⁰⁻¹³. This approach is distinct because nonlinear light-matter interactions require high-power lasers, whereas low-power continuous wave lasers have been employed for linear computations. Platforms like integrated meshes of Mach Zehnder Interferometers³, diffractive neural networks^{6,14-15}, micro-ring resonators^{7,16}, and free space vector matrix multipliers^{5,17} have facilitated linear calculations. However, for nonlinear computations, optoelectronic nonlinearity or electronic computation has been relied upon, resulting in limitations such as non-programable optoelectronic nonlinearity and high energy consumption. Therefore, there is a need to find a low power solution to implement non-linear operations in the optical domain in order to fully harness the low power computing potential offered inherently by linear optics.

The Ozcan group has introduced an approach to ONNs through the utilization of successive spatially engineered transmissive diffractive layers, employing additive manufacturing techniques¹⁵. These deep learning-enabled multi-layer diffractive processors enable computation by facilitating the propagation of free-space light through a sequence of structured passive scattering surfaces. This optical processing technique leverages the three-dimensional connectivity between nodes in consecutive layers, achieved via diffraction, thereby providing a path to scalability¹⁸. However, one limitation of this approach is that the nonlinearity is limited to the square law detection at the output which limits the realization of complex ONNs.

Another avenue that can be explored is the relationship between the scattering potential and the scattered light. While at low intensity levels, the propagation of light through a scattering medium exhibits linearity in terms of the relation between input and output light field, the output light can have a nonlinear dependence on the data encoded in the scattering potential. This form of nonlinearity is referred to as structural nonlinearity, and it has been investigated by a separate research group through the use of multiple scatterings within an integrating sphere¹⁹.

In this paper, we present a programmable framework called nonlinear Processing with only Linear Optics (nPOLO) for the all-optical realization of neural networks using a low-power continuous wave laser and diffractive layers. The nPOLO framework enables simultaneous linear and nonlinear operations within the optical domain. In this way, nPOLO unifies multi-layer light modulation and structural nonlinearity such that

the collective impact of data modulated layers on propagating light generates high order nonlinear transform of the data. Data is repetitively embedded into the modulation layers, combined with trainable parameters that enable the desired relationship (linear and nonlinear) between the data and the output field. Our results demonstrate that increasing the number of layers and data repetitions leads to the generation of higher-order nonlinearities, such as polynomial expansions, which include cross-terms among the different elements of the input data. To illustrate the effectiveness of data repetition, we conducted a comparative analysis of the performance obtained between repeating the data in each modulation layer and presenting the data only once. Our results demonstrate that, when both systems have an equal number of degrees of freedom in terms of the displayed pixels in modulation layers, the data repetition approach consistently achieves higher accuracy scores and exhibits improved robustness against experimental and simulated noise. Overall, our findings showcase the ability of the nPOLO framework to synthesize a learnable linear and non-linear data transform in a hybrid optical-digital neural network using only low power continuous wave light.

nPOLO framework

The core of the nPOLO technique involves utilizing multiple data planes that are evenly spaced apart. The physical implementation of nPOLO includes a liquid crystal Spatial Light Modulator (SLM) and a mirror positioned opposite to it, allowing the simultaneous display of multiple modulation planes on a single SLM device. This configuration forms a multi-bounce single pass cavity, where each plane serves as a thin element that modulates the phase of light as it propagates progressively from one plane to the next. Fig. 1 provides a visual representation of nPOLO. We introduce trainable parameters to program the transformation for executing specific tasks. These trainable parameters, in the form of scaling and bias, are applied to each pixel value of the data presented on the modulation layers. These parameters are trained digitally via a computer model (see Methods). Once the desired nonlinear transformation is achieved in the computer, the parameters are applied to the multiple layers (adjacent planes on the SLM) in the experimental setup, resulting in an intensity pattern that is recorded by a camera. Subsequently, a compact representation of the recorded camera pattern is obtained through average pooling, resulting in a 2D matrix of values such as a 4-by-4 or an 8-by-8 grid. This compact representation is then fed into a digital linear classifier, which processes the data via a single fully connected linear layer, thereby producing the final classification results.

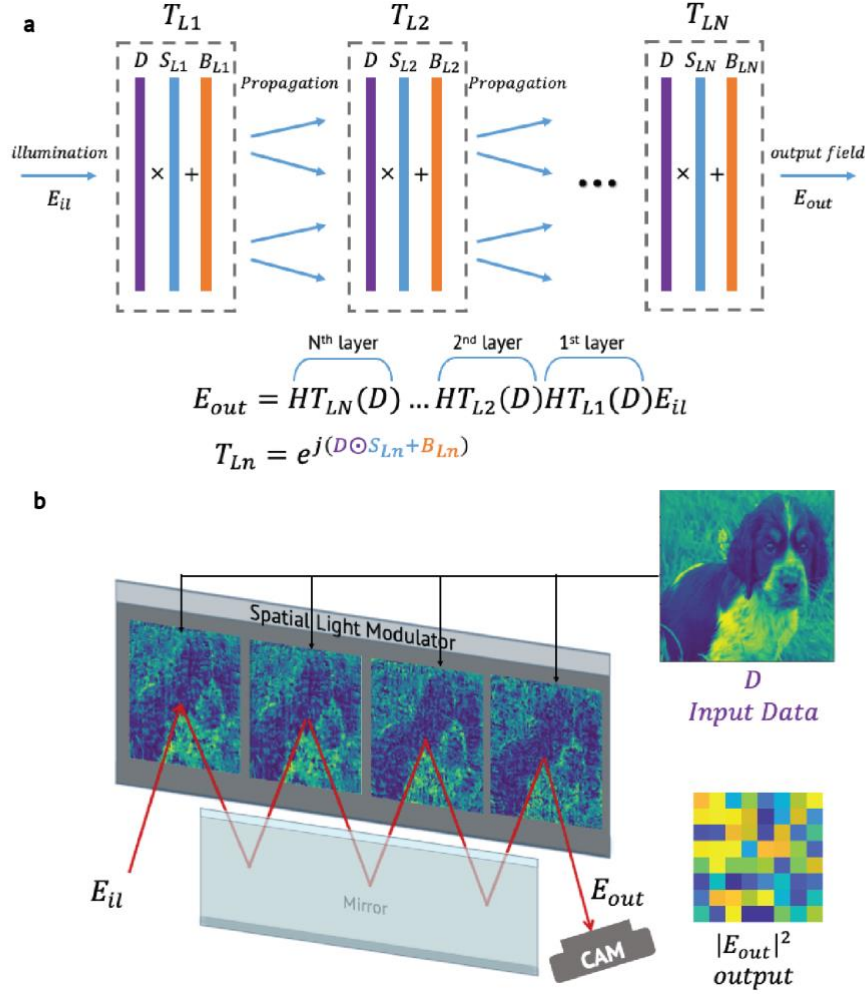


Figure 1. The framework of nPOLO a) The computation scheme is depicted, showcasing multiple modulation layers (T_{Ln}) within the framework. The data is presented on these layers, accompanied by trainable scaling and bias parameters to optimize the transformation. b) The physical implementation nPOLO, featuring a single pass multi-bounce cavity configuration. This implementation consists of a Spatial Light Modulator (SLM) and a mirror, positioned in a way that enables the realization of consecutive layers on the SLM side by side. The propagation distance is determined by the reflection from the mirror, allowing the light to propagate between the layers. Output light is captured with a camera.

By increasing the number of layers i.e. adjacent planes on the SLM, one can assess the impact of the polynomial expansion resulting from structural nonlinearity. However, the increase in the number of layers also leads to an increase in the system's degrees of freedom and space-bandwidth product. Therefore, we devised an alternative comparison experiment to mitigate these effects. In our experiments, we maintained the same number of layers and pixels but modified the data allocation. Specifically, we initially incorporated the data only in the first layer, while the subsequent layers consisted exclusively of trainable bias parameters without any data or scaling parameters. To evaluate the performance of the nPOLO framework, we conducted

experiments using the Imagenette, Fashion MNIST and Digit MNIST datasets²⁰⁻²². The obtained numerical and experimental results are provided in Fig. 2.

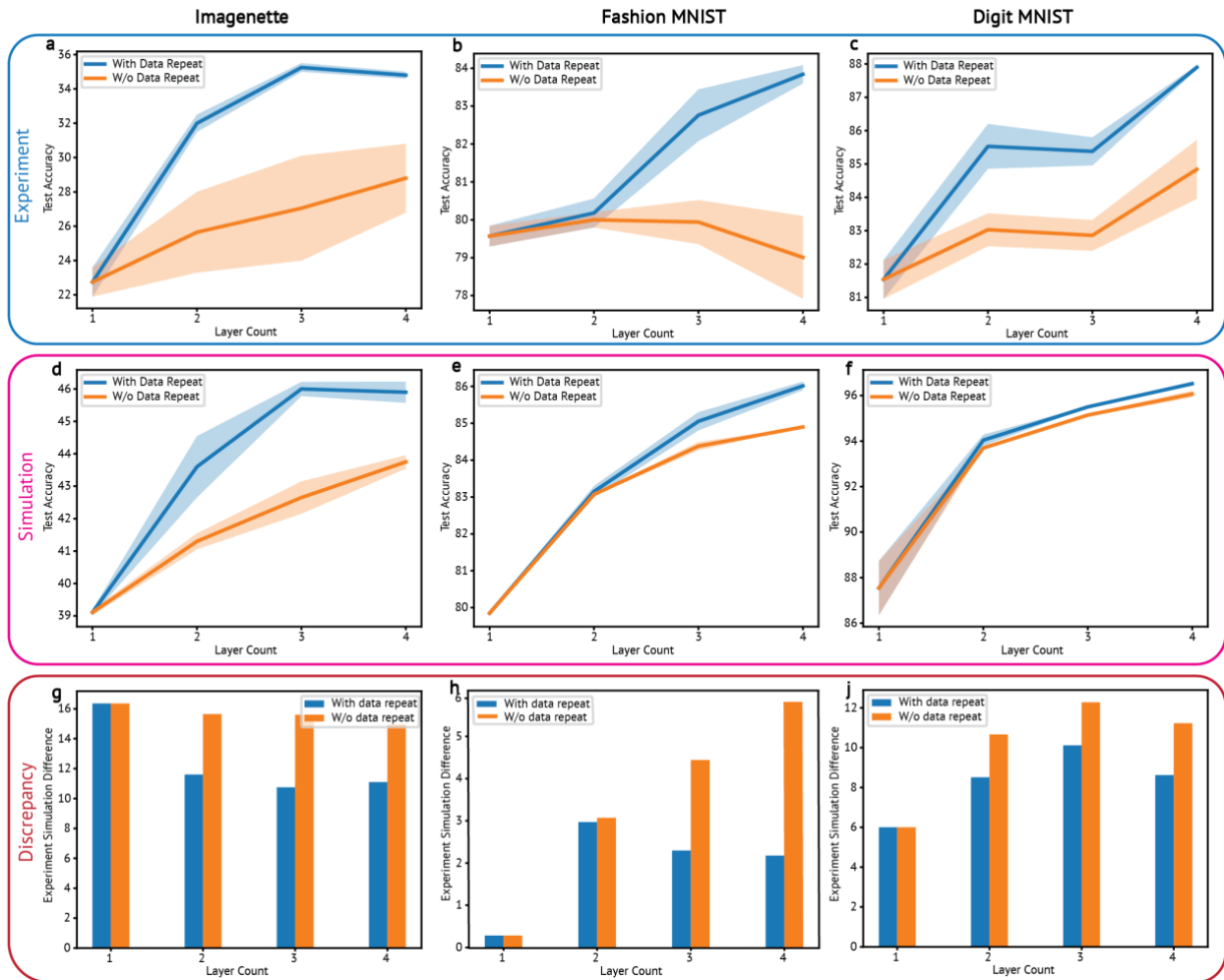


Figure 2 showcases the classification accuracy results obtained for the Imagenette (a,d,g), Fashion MNIST (b,e,h) and Digit MNIST (c,f,j) datasets, comparing two different schemas: one with "data repeat" and one without. The layer count (N) is varied from one to four for both schemas. Each configuration is trained independently, resulting in layer masks that are applied to the Spatial Light Modulator (SLM) as phase masks. a, b, c) The experimentally obtained test accuracies for all datasets are displayed, representing the performance with and without structural nonlinearity. d, e, f) Test accuracies of corresponding simulations are plotted for both schemas likewise in experiments. g, h, j) The accuracy difference between experimental and simulated results are shown as bar plot for varying layer number with and without data repeat.

For clarity, we provide examples of the displayed masks in Fig. 3 "with data repeat" and "without data repeat" configurations using an example from the Fashion MNIST and Imagenette datasets with four modulation layers. Also see the Supplementary Fig. 1 for the comparative depiction of parameter allocation. The trainable

parameters were optimized by computer simulation, wherein the physical light propagation was modeled using the Beam Propagation Method (BPM).

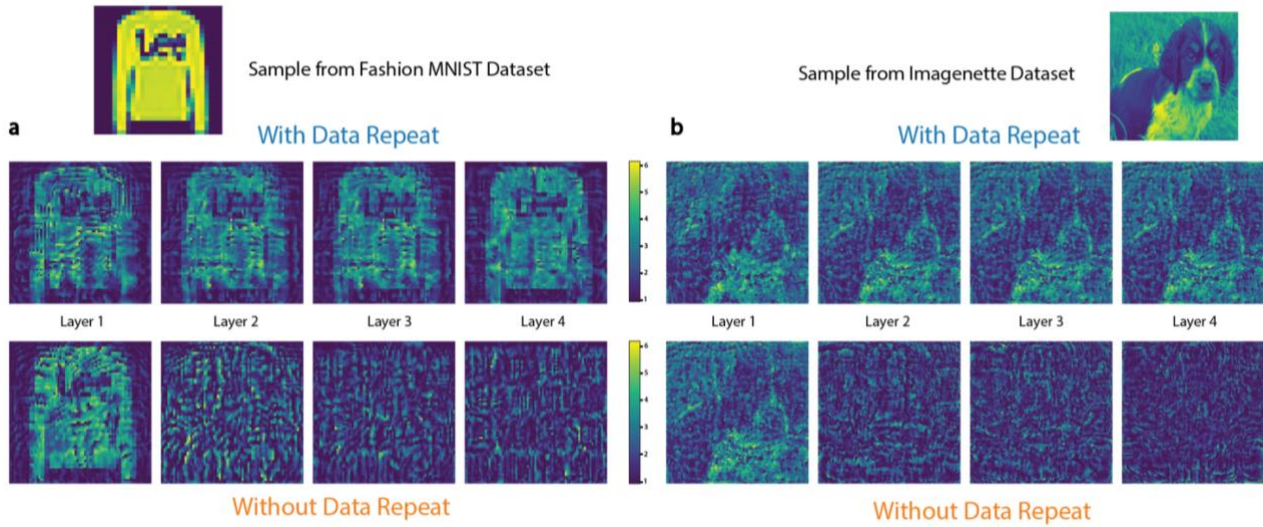


Figure 3. Samples of trained layer masks to be displayed on SLM for Fashion MNIST and Imagenette. a) Presents an example sample from the Fashion MNIST dataset alongside its corresponding layer masks, combined with trainable parameters, according to both schemas. The color code utilized represents the phase modulation ranging from 0 to 2π . Similarly, panel (b) showcases an example sample from the Imagenette dataset and its corresponding layer masks combined with trainable parameters for both schemas.

Since BPM consists of differentiable calculation steps, the error can be backpropagated to the trainable parameters, and they are optimized using stochastic gradient descent. In Fig. 4, we present the training scheme used, in which the digital model of the optical system and the digital classifier were co-trained for the classification tasks. By following this co-training approach, we obtained scaling and bias masks for different layer configurations, ranging from layer $N=1$ to layer $N=4$, both with and without data repetition. It is important to note that in the case of a single layer ($N=1$), both data repetition options are equivalent, as we only had a single layer available to introduce the data.

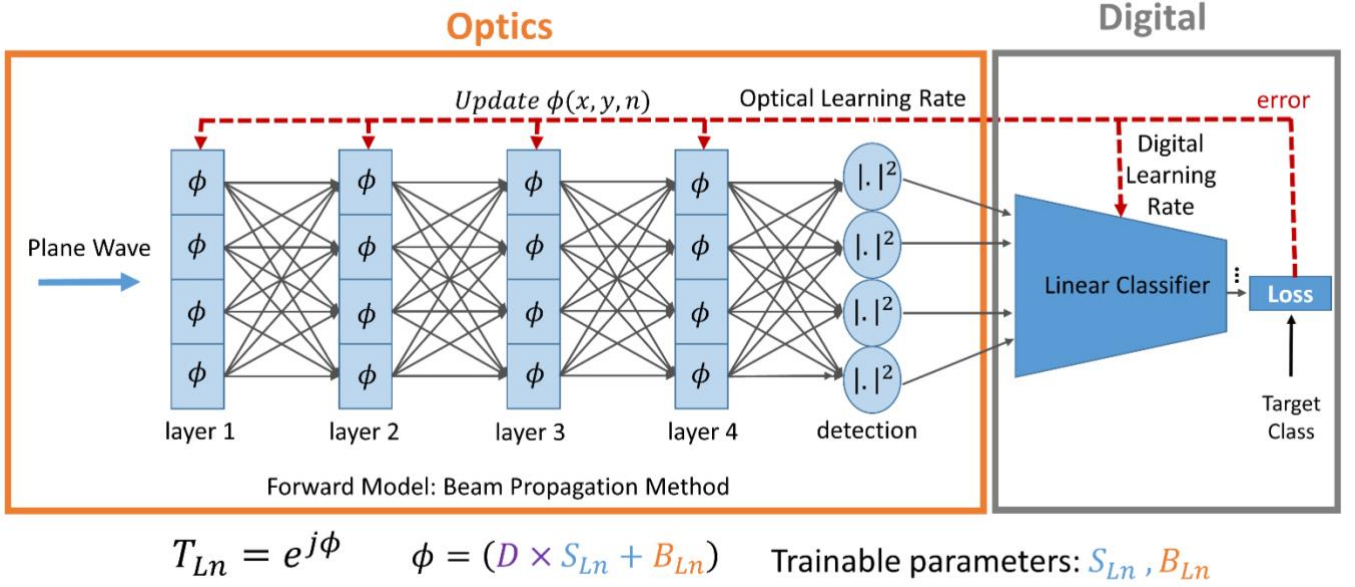


Figure 4. Co-training of optical trainable parameters and digital trainable parameters. Simulation model of four-layer system based is built by beam propagation method, where layers are composed of trainable parameters (S_{Ln} and B_{Ln}). Training of optical layers and linear classifier is performed simultaneously using separate learning rates.

Our experimental findings in Fig. 2-a, b and c consistently demonstrated that when data was repeated across multiple layers, we achieved higher classification accuracy compared to configurations without data repetition. Moreover, increasing the number of layers also contributed to improved accuracy. We also observed that when the number of layers was held constant, eliminating data repetition led to a reduction in accuracy. These results highlight the contribution of both higher order optical nonlinearities generated via data repetition and the number of layers in maximizing the classification task performance. We observed a similar trend in our simulations while calculating the trainable parameters (see Fig. 2-d,e,f). Both experimental and simulated results validate the contribution of the nPOLO framework. However, it is worth mentioning that the experimental accuracies were lower than the simulated ones. Fig. 2-g,h,j illustrate the accuracy difference between simulations and experiments in all three datasets. The decrease in accuracy is less pronounced in cases involving data repetition compared to those without. We attribute this discrepancy to imperfections between the simulated model and the physical implementation, such as the non-ideal phase response of the SLM and beam tilt, among others. As a preliminary study to assess digital counterpart of the nPOLO for these tasks, we trained simple convolutional neural networks and obtained comparable performance, see Supplementary Result 1.

Discussion

As described in the Methods section, the fixed and complex connectivity provided by free space propagation between each layer does not guarantee the extraction of useful representations. To address this limitation, we introduced trainable scaling and bias parameters for the pixel values of the displayed samples. It is important to note that this approach serves as a simple scheme for tuning the transformation. Future studies could explore alternative approaches, such as using convolutional kernels or eigenmodes of the optical system as trainable parameters, similar to investigations conducted for fiber-based optical learning machines²³. During the final stage of this work, we became aware of an independent and different approach to perform passive optical non-linearity, exploiting reflections inside a disordered cavity. By investigating these methods, we may further exploit the effects of higher-order nonlinearities.

Furthermore, we observed that the contribution of structural nonlinearity became more pronounced when dealing with more challenging classification tasks. The impact of using repeated data versus not using repeated data was more significant for Imagenette compared to Digit MNIST. This disparity arises because Digit MNIST represents an easier task, and the structural nonlinearity becomes redundant in the presence of detection nonlinearity.

Another notable observation is the increased robustness of data repetition across multiple layers against noise. We initially noticed this phenomenon during experiments conducted on different datasets and layer configurations. To further investigate this, we introduced increasing levels of noise in BPM simulations while keeping the trained masks fixed (see Supplementary Discussion 1). Gradually increasing the simulated noise level, we observed that the layers with data repetition exhibited greater robustness compared to the configurations without data repetition. The latter experienced a more rapid drop in accuracy, consistent with the experimental results. This finding strengthens the argument for the noise robustness of the data repetition scheme, as we have empirical data from both experiments and simulations. One possible explanation for this phenomenon is that by introducing the data multiple times, we create multiple paths from the input data to the output plane, resulting in not only higher polynomial orders but also cross-terms that couple with different optical paths and reach the detector plane. The existence of multiple routes for highlighting useful features in the output plane may make the data repetition scheme less susceptible to noise.

Overall, the nPOLO framework presents a novel approach for generating optical nonlinearity using low-power optical devices, eliminating the need for electronic components to achieve higher orders of nonlinearity. Furthermore, the introduction of data repetition to generate polynomial nonlinearities enhances robustness against noise. These characteristics make nPOLO a promising platform for realizing optical neural networks.

Methods

Derivation of nonlinear response in nPOLO

Without loss of generality, let us assume that we have an optical system that has an input aperture and output aperture that are discretized/sampled by the same number of K pixels where this optical system comprises of N modulation layers that are equally spaced from each other. The system response for a single modulation layer is the following:

$$o = P2 \times T \times P1 \times i$$

Where o is the $K \times 1$ output vector (Electric field), i is the $K \times 1$ input vector (Electric field), $P1$ is the propagation matrix representing the diffraction from the input aperture to the modulation layer, $P2$ is the propagation matrix representing the diffraction from the modulation layer to the output aperture, and T is the modulation matrix. Assuming the same number of K pixels in the modulation layer as in the input/output apertures, T becomes a diagonal matrix with size $K \times K$. We use a Toeplitz matrix to represent diffraction for an arbitrary distance. For simplicity, we assume that the modulation layer coincides with the input aperture, which makes $P1$ a unity matrix and the input field is a plane wave, which makes i a vector of ones. For the subsequent propagation matrices, we will assume them to be the same and denote as H . Then, for a single modulation layer for the explained configuration, we have:

$$\begin{bmatrix} o_1 \\ \vdots \\ o_K \end{bmatrix} = \begin{bmatrix} \sum_{k=1}^K h_{1k} t_k \\ \vdots \\ \sum_{k=1}^K h_{Kk} t_k \end{bmatrix}$$

Where h_{ij} are coefficients of the propagation matrix H . If we repeat this process N times for N modulation layers, we have:

$$\begin{bmatrix} o_1 \\ \vdots \\ o_K \end{bmatrix} = \begin{bmatrix} \prod_{n=1}^N \left(\sum_{k=1}^K h_{1k} t_k \right) \\ \vdots \\ \prod_{n=1}^N \left(\sum_{k=1}^K h_{Kk} t_k \right) \end{bmatrix}$$

From this relationship, we can see that repeating the modulation layers with the same coefficients yields cross-terms and polynomial orders of the coefficients belonging to the modulation layer. Hence, when the data is introduced in the modulation layers, we end up with the nonlinear relationship along with the generated cross-terms that yield additional features. In the supplementary material, we further analyze the outcomes when the modulation layer provides complex modulation or phase-only modulation along with the difference between field detection and intensity detection. When we have phase-only modulation, the multiplicative nature of the repetition causes a linear relationship between the modulation layers and the output field. Hence intensity detection is required to establish a nonlinear response that results in a polynomial expansion of the sinusoidal terms further enriching the nonlinear mixing of the introduced data in multiple modulation layers (see Supplementary Discussion 2).

Digital training

We previously demonstrated an optimization method by inverting the intended use of Learning Tomography, which is a method to reconstruct 3D phase objects from experimental recordings of 2D projections²⁴. The forward model in the optimization is the beam propagation method (BPM). The iterative error reduction scheme and the multilayer structure of the BPM resembles a multilayer neural network. Therefore, this method is referred to as Learning Tomography. We showed that instead of imaging an object, we can reconstruct the 3D structure that performs the desired task as defined by its input-output functionality²⁵. To establish the target functionality, the 3D phase modulation, either through a continuous medium or multiple planes, and the scattered field caused by the phase modulation must be accurately modeled. Unlike conventional reconstruction algorithms that rely on first-order approximations, LT incorporates higher-order scattering effects by employing BPM. The LT algorithm involves an iterative reconstruction process using the forward model, along with the constraints arising from experimental considerations such as the pixel pitch of the SLM. In this study, we adapted this approach presented in the ref²⁵, where additional details can be found, to generate scaling and bias parameters for demonstrated classification tasks. The output intensity pattern of the forward model is average pooled to yield a 4-by-4 matrix for each sample of Fashion MNIST dataset and an 8-by-8 matrix for each sample of the Imagenette dataset. These matrices are flattened to act as an input layer of a digital classifier that has 10 output neurons for each class of the datasets without any hidden

layer and nonlinear activation function. The trainable parameters employed in the BPM model and digital classifier are co-trained by a continuous error backpropagation where different learning rates are assigned to digital weights (i.e., 10^{-4}) and optical scaling and bias parameters (i.e., 10^{-3}) using categorical cross entropy as the loss function. We used batch learning with a batch size of 20 and a random shuffle in every batch. PyTorch libraries are used for the whole training process.

Note that, as explained in the experimental setup section, we use 300 by 300 pixels on SLM for each modulation layer whereas the Fashion MNIST and the Digit MNIST dataset samples contain 28 by 28 pixels and Imagenette dataset samples contain 320 by 320 pixels. For the Fashion MNIST and the Digit MNIST datasets, we used 4 by 4 superpixels on SLM, yielding 75 by 75 pixels for accepting and assigning trainable parameters, which means that we assign 11250 parameters (scaling and bias) per modulation layer. We accordingly linearly up-sampled the samples of those datasets to 75 by 75. For the Imagenette dataset, we linearly down-sampled the samples to 300 by 300 and did not use any superpixels on SLM meaning that we used 300 by 300 pixels for accepting and assigning trainable parameters, which means that we assign 180000 parameters (scaling and bias) per modulation layer.

Experimental setup

A photograph showcasing our optical setup is presented in Supplementary Figure 3. In our experiments, we employed a continuous wave Solstis M2 laser operating at a wavelength of $\lambda = 850 \text{ nm}$. The mirror we used has a width of 11 mm, providing ample space for the four reflections. To deliver the beam to the SLM, we implemented 4f imaging to relay the beam reflected from a digital micromirror device (DMD). The use of a DMD offered the advantage of flexible beam sizing. Specifically, we configured the beam shape as a square with a side length of 2.4 mm, corresponding to a 300 by 300 pixel area on the SLM. It is worth noting that the SLM utilized in our setup has an $\Lambda = 8 \mu\text{m}$ pixel pitch. To construct a multi-bounce cavity, we utilized a Holoeye Pluto Spatial Light Modulator (SLM) and positioned the mirror at a distance of $d = 15.2 \text{ mm}$ from the SLM screen. This distance is set so that diffraction from one corner pixel of a layer can reach to the opposite corner of the subsequent layer ($d \times \lambda/\Lambda \geq 2.4 \text{ mm}$). Which enables all to all pixel connectivity. This configuration allowed the input beam to undergo four reflections from the mirror. After the fourth bounce, the beam on the SLM is magnified by a factor of 1.2, and the resulting output intensity is detected by a CMOS camera with a pixel pitch of $3.45 \mu\text{m}$. The corresponding beam in the camera occupies an area of 834 by 834 pixels. During image acquisition, we applied average pooling to resize the obtained images to either 4 by 4 or 8 by 8 dimensions. For the Imagenette dataset, we used the whole training and test samples as originally prepared. For the Digit and Fashion MNIST datasets, we used the whole training set (60000 samples) for the simulations however we used the first 10000 samples for the re-training of digital weights after the experiments and we used the first 2500 samples of the test set for blind testing of the experimental results.

References

1. Denz, C. Optical neural networks. Springer Science & Business Media, (2013).
2. Wetzstein, G., Ozcan, A., Gigan, S., Fan, S., Englund, D., Soljačić, M., ... & Psaltis, D. "Inference in artificial intelligence with deep optics and photonics." *Nature* 588.7836, 39-47 (2020).
3. Shen, Y., et al. "Deep learning with coherent nanophotonic circuits." *Nature photonics* 11, no. 7 441-446 (2017)
4. Feldmann, J., Youngblood, N., Wright, C. D., Bhaskaran, H. & Pernice, W. H. P. All-optical spiking neurosynaptic networks with self-learning capabilities. *Nature* 569, 208–214 (2019).
5. Farhat, N. H., Psaltis, D., Prata, A. & Paek, E. Optical implementation of the Hopfield model. *Appl. Opt.* 24, 1469–1475 (1985).
6. Lin, Xing, Yair Rivenson, Nezih T. Yardimci, Muhammed Veli, Yi Luo, Mona Jarrahi, and Aydogan Ozcan. "All-optical machine learning using diffractive deep neural networks." *Science* 361, no. 6406 1004-1008 (2018).
7. Tait, A. N. et al. Neuromorphic photonic networks using silicon photonic weight banks. *Sci. Rep.* 7, 7430 (2017).
8. Tanaka, G. et al. Recent advances in physical reservoir computing: A review. *Neural Networks* vol. 115 100–123 (2019).
9. Gao, C., Gaur, P., Rubin, S., & Fainman, Y. (2022). Thin liquid film as an optical nonlinear-nonlocal medium and memory element in integrated optofluidic reservoir computer. *Advanced Photonics*, 4(4), 046005.
10. Teğin, U., Yıldırım, M., Oğuz, İ., Moser, C. & Psaltis, D. Scalable optical learning operator. *Nat. Comput. Sci.* 2021 18 1, 542–549 (2021).
11. Wright, L. G. et al. Deep physical neural networks trained with backpropagation. *Nature* 601, 549–555 (2022).
12. Zhou, T., Scalzo, F. & Jalali, B. Nonlinear Schrödinger Kernel for Hardware Acceleration of Machine Learning. *J. Light. Technol.* 40, 1308–1319 (2022).
13. Yildirim, M., Oguz, I., Kaufmann, F., Escalé, M. R., Grange, R., Psaltis, D., & Moser, C. Nonlinear optical data transformer for machine learning. *arXiv preprint arXiv:2208.09398* (2022).
14. Zhou, T. et al. Large-scale neuromorphic optoelectronic computing with a reconfigurable diffractive processing unit. *Nat. Photonics* 15, 367–373 (2021).
15. Kulce, O., Deniz, M., Yair, R., & Aydogan O. "All-optical synthesis of an arbitrary linear transformation using diffractive surfaces." *Light: Science & Applications* 10, no. 1 196 (2021).
16. Huang, C. et al. Demonstration of scalable microring weight bank control for large-scale photonic integrated circuits. *APL Photonics* 5, 040803 (2020).
17. Spall, J., Guo, X., Barrett, T. D. & Lvovsky, A. I. Fully reconfigurable coherent optical vector-matrix multiplication. *Opt. Lett.* 45, 5752 (2020).

18. Dinc, N. U., Saba, A., Madrid-Wolff, J., Gigli, C., Boniface, A., Moser, C., & Psaltis, D. From 3D to 2D and back again. *Nanophotonics*, 12(5), 777-793. (2023).
19. Eliezer, Y., Ruhmair, U., Wisiol, N., Bittner, S., & Cao, H. Exploiting structural nonlinearity of a reconfigurable multiple-scattering system. *arXiv preprint arXiv:2208.08906*. (2022).
20. Xiao, H., Rasul, K., & Vollgraf, R. (2017). Fashion-mnist: a novel image dataset for benchmarking machine learning algorithms. *arXiv preprint arXiv:1708.07747*. (2017).
21. Howard, J., & Gugger, S. Fastai: A layered API for deep learning. *Information*, 11(2), 108. (2020).
22. Y. LeCun, L. Bottou, Y. Bengio, and P. Haffner. "Gradient-based learning applied to document recognition." *Proceedings of the IEEE*, 86(11):2278-2324, November 1998.
23. Oguz, I., Hsieh, J. L., Dinc, N. U., Teğin, U., Yildirim, M., Gigli, C., ... & Psaltis, D. (2022). Programming nonlinear propagation for efficient optical learning machines. *arXiv preprint arXiv:2208.04951*.
24. U. S. Kamilov, I. N. Papadopoulos, M. H. Shoreh, et al., "Learning approach to optical tomography," *Optica*, vol. 2, pp. 517–22, <https://doi.org/10.1364/optica.2.000517>. (2015).
25. Dinc, N. U., Lim, J., Kakkava, E., Moser, C., & Psaltis, D. Computer generated optical volume elements by additive manufacturing. *Nanophotonics*, 9(13), 4173-4181. (2020).

Data availability

The data that support the plots within this article and other findings of this study are available from the corresponding author upon reasonable request.

Code availability

All relevant code is available from the corresponding author upon reasonable request.

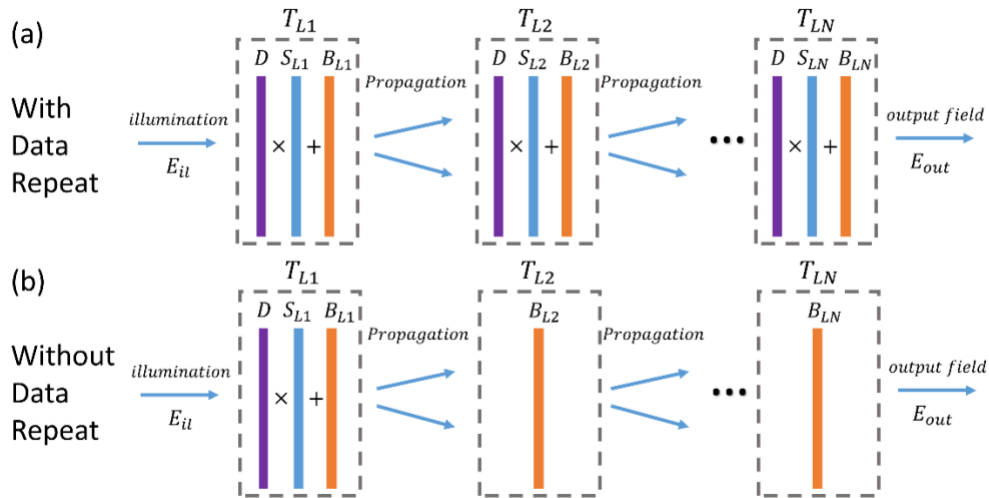
Author contributions

M.Y., N.U.D., D.P., and C.M. conceived and initiated the project. N.U.D. provided the first version of numerical training module. M.Y. and N.U.D. modified the training scheme according to the needs of this project. M.Y., N.U.D., and I.O. worked on the experimental setup and used datasets. All the authors contributed to the guidance of the experiments and the discussion of the results. M.Y. and N.U.D. prepared the first draft of the manuscript. All the authors revised the manuscript. D.P. and C.M. supervised the project.

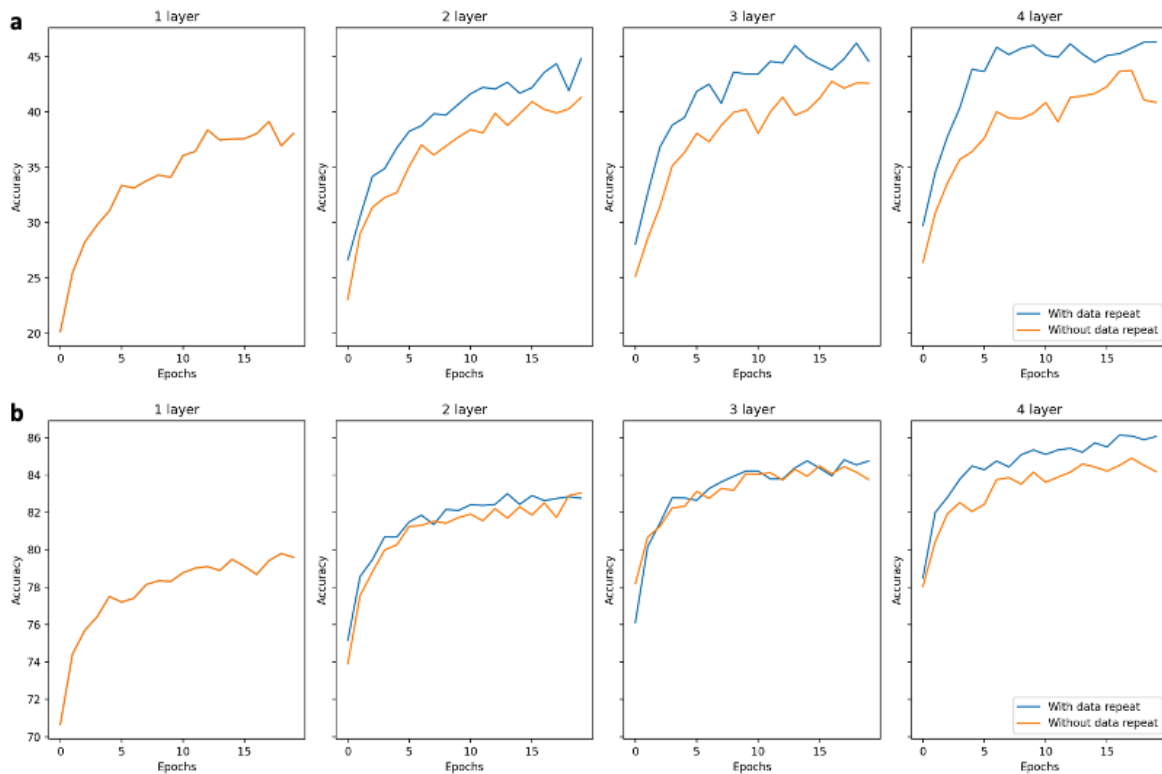
Competing interests

The authors declare no competing interests.

Supplementary Material

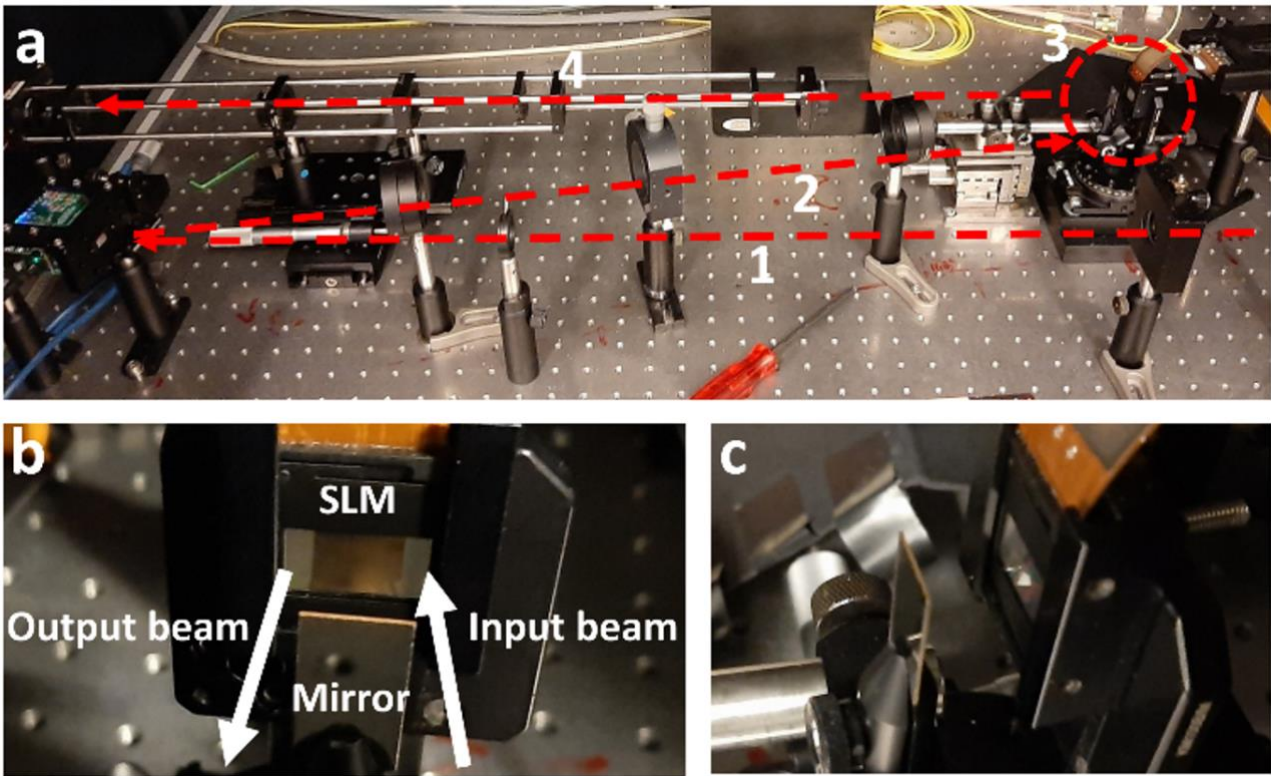


Supplementary Figure 1. Comparison scheme to observe the effect of structural nonlinearity with equivalent systems in terms of space-bandwidth product. a) Cascaded modulation layers where each layer comprises the input data as given in Figure 1a as well. b) Cascaded modulation layers where only the first layer comprises the input data and the consecutive layers contain trainable bias parameters.



Supplementary Figure 2 demonstrates the test accuracy results obtained during training of the Imagenette (a) and Fashion MNIST (b) datasets on two different schemas: one with "data repeat"

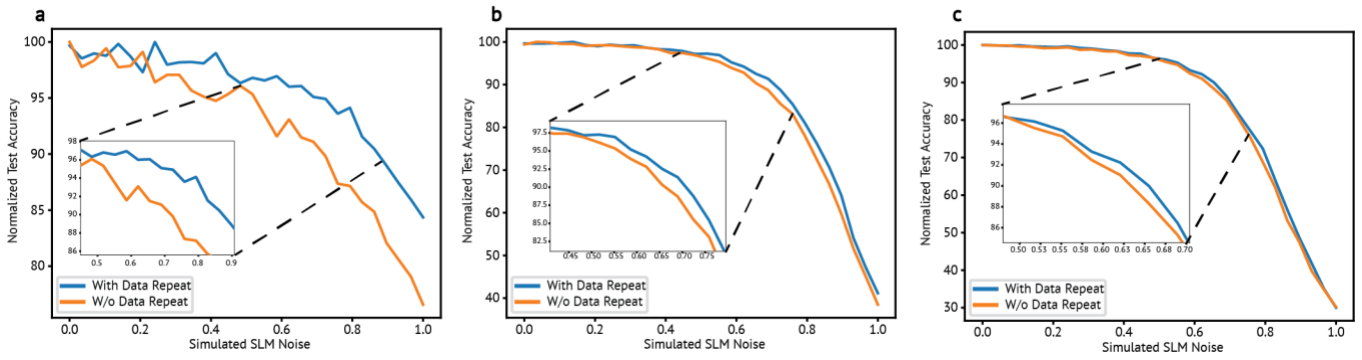
and one without. Note that, one layer corresponds to same configuration for both schemas. Each configuration is trained for 20 epochs.



Supplementary Figure 3 demonstrates the experimental setup. a) The experimental setup. 1-collimated laser beam path, 2-a Digital Micromirror Device (DMD) emulates input aperture and a 4F imaging system relays the light into multi-bounce cavity, 3-multi-bounce cavity, 4-another 4F imaging system relays the output of the multi-bounce cavity on a camera. b) Front-view of the multi-bounce cavity in the setup c) side-view of the multi-bounce cavity.

Supplementary Discussion 1: Numerical study to probe noise robustness

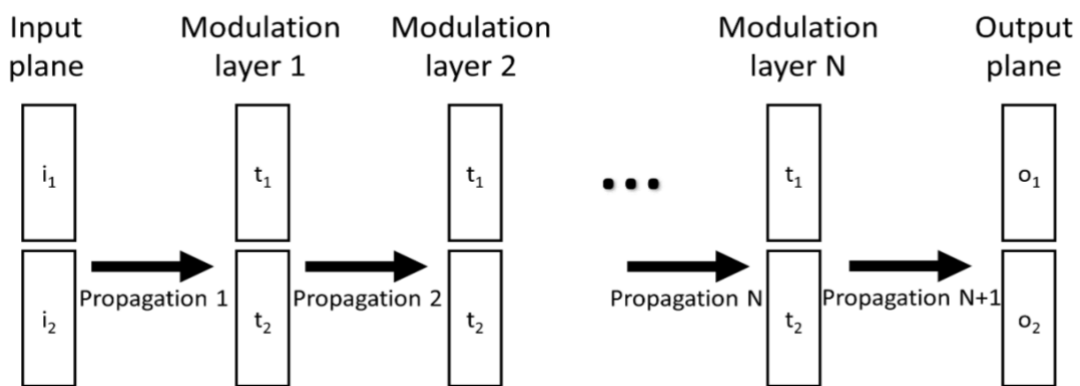
To investigate the influence of phase noise on SLM (Spatial Light Modulator), we conducted simulations by introducing random additive phase noise to the trainable parameters. We applied the forward model to all three datasets for various the levels of phase noise. The noise were randomly generated from a normal distribution and applied to every pixel of the four layers. Subsequently, we determined the output accuracy based on the simulated outputs affected by the introduced noise. Supplementary Figure 4 demonstrates that as the strength of the noise increases, the accuracy drop of without data repetition occurs more rapidly. This numerical analysis corroborates the findings from our experimental observations.



Supplementary Figure 4 illustrates the effect of phase noise on pixels. The plots depict the test accuracy drop as the phase noise on the Spatial Light Modulator (SLM) is incrementally increased from zero to one (corresponding to 2π), both for the cases with data repetition and without data repetition. The obtained test accuracies are normalized to the scenario where the phase noise is zero. Panels a, b, and c correspond to the datasets: Imagenette, Fashion MNIST, and Digit MNIST, respectively. The insets provide a zoomed view of the difference between the cases with data repetition and without data repetition.

Supplementary Discussion 2: Derivation of nonlinear response for 2-pixel layers

We present an analysis of a simplified optical system where each plane/layer consists of two pixels (see Supplementary Discussion 2 - Figure 1) and a propagation step whose system response is expressed by a matrix with linear coefficients. The generalization of this analysis to an arbitrary number of pixels in each layer is straightforward. We provide the investigation for Modulation layer number $N=1$, $N=2$, and $N=3$ for ease of explanation and the conclusions are valid for arbitrary N by inductive reasoning.



Supplementary Discussion 2 - Figure 1: sketch of the simplified optical system where each plane/layer consists of two pixels.

The system response for Modulation layer $N=1$ is the following:

$$o = P2 \times T \times P1 \times i$$

Where o is the output vector (Electric field), i is the input vector (Electric field), $P1$ is the propagation matrix 1, $P2$ is the propagation matrix 2, and T is the modulation matrix. For $P1$, we assume zero propagation for simplicity without losing generality and for $P2$ we use a Toeplitz matrix to represent diffraction for an arbitrary distance. For a two-pixel per layer system we simply have the following:

$$P1 = \begin{bmatrix} 1 & 0 \\ 0 & 1 \end{bmatrix}$$

$$P2 = \begin{bmatrix} h_{11} & h_{12} \\ h_{21} & h_{22} \end{bmatrix}$$

$$T = \begin{bmatrix} t_1 & 0 \\ 0 & t_2 \end{bmatrix}$$

Hence:

$$\begin{bmatrix} o_1 \\ o_2 \end{bmatrix} = \begin{bmatrix} h_{11} & h_{12} \\ h_{21} & h_{22} \end{bmatrix} \begin{bmatrix} t_1 & 0 \\ 0 & t_2 \end{bmatrix} \begin{bmatrix} i_1 \\ i_2 \end{bmatrix}$$

And we have:

$$\begin{bmatrix} o_1 \\ o_2 \end{bmatrix} = \begin{bmatrix} h_{11}t_1i_1 + h_{12}t_2i_2 \\ h_{21}t_1i_1 + h_{22}t_2i_2 \end{bmatrix}$$

Following similar steps for Modulation layer $N=2$ (assuming $P3=P2$ without loss of generality). Note that the data in layer $N=2$ is the same as layer $N=1$.

$$\begin{bmatrix} o_1 \\ o_2 \end{bmatrix} = \begin{bmatrix} h_{11} & h_{12} \\ h_{21} & h_{22} \end{bmatrix} \begin{bmatrix} t_1 & 0 \\ 0 & t_2 \end{bmatrix} \begin{bmatrix} h_{11}t_1i_1 + h_{12}t_2i_2 \\ h_{21}t_1i_1 + h_{22}t_2i_2 \end{bmatrix}$$

$$\begin{bmatrix} o_1 \\ o_2 \end{bmatrix} = \begin{bmatrix} h_{11}^2t_1^2i_1 + h_{11}h_{12}t_2t_1i_2 + h_{12}h_{21}t_1t_2i_1 + h_{12}h_{22}t_2^2i_2 \\ h_{21}h_{11}t_1^2i_1 + h_{21}h_{12}t_2t_1i_2 + h_{22}h_{21}t_1t_2i_1 + h_{22}^2t_2^2i_2 \end{bmatrix}$$

Hence, we reach a nonlinear relationship between the output field o_1, o_2 and the data plane t_1, t_2 . When intensity detection is employed as the acquisition method, the obtained output will be the absolute square of the field, providing a 4th order polynomial expansion of the parameters inserted in the modulation layers for

the specific case of 2 layers (N=2). Clearly, when data is introduced in the modulation layers, we obtain a nonlinear processing of the data at the output plane either by detecting the field (by a holographic recording) and/or the intensity (by a simple detector, which can be CMOS, CCD, etc.). The input field i can be a programming parameter to change the effective transform. For simplicity, we will continue with a plane wave input without loss of generality:

$$\begin{bmatrix} i_1 \\ i_2 \end{bmatrix} = \begin{bmatrix} 1 \\ 1 \end{bmatrix}$$

For a phase-only modulation, we have the following relation for the modulation terms:

$$t_i = e^{j\phi_i} \text{ where } j = \sqrt{-1}.$$

In this case, the data becomes ϕ_i . Then we have:

$$\begin{bmatrix} o_1 \\ o_2 \end{bmatrix} = \begin{bmatrix} h_{11}^2 e^{j2\phi_1} + h_{11}h_{12}e^{j(\phi_1+\phi_2)} + h_{12}h_{21}e^{j(\phi_1+\phi_2)} + h_{12}h_{22}e^{j2\phi_2} \\ h_{21}h_{11}e^{j2\phi_1} + h_{21}h_{12}e^{j(\phi_1+\phi_2)} + h_{22}h_{21}e^{j(\phi_1+\phi_2)} + h_{22}^2 e^{j2\phi_2} \end{bmatrix}$$

In the above expression, there is no polynomial expansion of the data at the output electric field. However, when we detect the intensity, we obtain:

$$\begin{aligned} \begin{bmatrix} I_1 \\ I_2 \end{bmatrix} &= \begin{bmatrix} |o_1|^2 \\ |o_2|^2 \end{bmatrix} = \begin{bmatrix} \left| h_{11}^2 e^{j2\phi_1} + h_{11}h_{12}e^{j(\phi_1+\phi_2)} + h_{12}h_{21}e^{j(\phi_1+\phi_2)} + h_{12}h_{22}e^{j2\phi_2} \right|^2 \\ \left| h_{21}h_{11}e^{j2\phi_1} + h_{21}h_{12}e^{j(\phi_1+\phi_2)} + h_{22}h_{21}e^{j(\phi_1+\phi_2)} + h_{22}^2 e^{j2\phi_2} \right|^2 \end{bmatrix} \\ &= \begin{bmatrix} DC + C_1 \cos(\phi_1 - \phi_2 + \theta_1) + C_2 \cos(2(\phi_1 - \phi_2 + \theta_2)) \\ DC + C_3 \cos(\phi_1 - \phi_2 + \theta_3) + C_4 \cos(2(\phi_1 - \phi_2 + \theta_4)) \end{bmatrix} \end{aligned}$$

In the above expression, the DC term refers to the grouping of the terms that do not depend on the SLM phase pattern ϕ_i . The constant terms C_i represent the electric field amplitude resulting from light propagation between layers. θ_i is the additional phase bias of the constants arriving from propagation matrix. The elements of the propagation matrix are complex valued. Note that the intensity detection yields cosine terms. The integer multiplier (the factor 2) in the second cosine term comes from the fact that there are two modulation layers. Note that this term has a polynomial expansion:

$$\cos(2\theta) = 2\cos^2(\theta) - 1$$

Hence, intensity detection provides the nonlinearity (cosine) and where the multiple modulation layers provide the polynomial expansion of the cosine term. Similarly, when adding a third modulation layer N=3, we have:

$$\begin{bmatrix} o_1 \\ o_2 \end{bmatrix} = \begin{bmatrix} h_{11}^3 t_1^3 + (h_{11}^2 h_{12} + 2h_{12} h_{21} h_{11}) t_2 t_1^2 + (h_{11} h_{12} h_{22} + h_{12}^2 h_{21} + h_{12} h_{21} h_{22}) t_1 t_2^2 + h_{12} h_{22}^2 t_2^3 \\ h_{21} h_{11}^2 t_1^3 + (h_{21} h_{11} h_{12} + h_{21}^2 h_{12} + h_{11} h_{21} h_{22}) t_2 t_1^2 + (h_{22}^2 h_{21} + 2h_{12} h_{21} h_{22}) t_1 t_2^2 + h_{22}^3 t_2^3 \end{bmatrix}$$

$$\begin{bmatrix} I_1 \\ I_2 \end{bmatrix} = \begin{bmatrix} DC + C_1 \cos(\phi_1 - \phi_2 + \theta_1) + C_2 \cos(2(\phi_1 - \phi_2 + \theta_2)) + C_3 \cos(3(\phi_1 - \phi_2 + \theta_3)) \\ DC + C_4 \cos(\phi_1 - \phi_2 + \theta_4) + C_5 \cos(2(\phi_1 - \phi_2 + \theta_5)) + C_6 \cos(3(\phi_1 - \phi_2 + \theta_6)) \end{bmatrix}$$

Noting that:

$$\cos(3\theta) = 4\cos^3(\theta) - 3\cos(\theta)$$

By induction, it is obvious that the polynomial expansion increases with the number of modulation layers N. In summary,

- Complex modulation (amplitude and phase) or with only amplitude modulation in the different layers yield a nonlinear relationship between the output field and the modulation even without intensity detection.
- Phase-only modulation in the different layers yield a nonlinear relationship between the output field and the modulation only when intensity detection is performed.

Essentially, the trainable parameters S_i , B_i that are added to each pixels of the data layers change the evaluation regime on the cosine polynomials. Hence, their effect is analogous to the nonlinear activation in deep neural networks.

Supplementary Result 1:

We trained convolutional neural networks (CNN) that can provide close performances to nPOLO accuracies obtained in simulations. Neural network details are provided for each dataset in the following.

Imagenette: Original dataset consists of 320 by 320 RGB images. Since in nPOLO we use grayscale images we have converted RGB to grayscale. Additionally, the size of images are rescaled to 128 by 128 because of memory considerations for digital networks. The same CNN architecture as LeNet-5¹ is used but fully connected layers differ in hidden unit size due to the input image size. In this way, hidden unit sizes are 13456, 1024 and 256. For the light CNN, 3 and 6 filters are used in first and second layers of convolutions, respectively. Corresponding hidden unit sizes are: 5046, 256 and 64.

Fashion and Digit MNIST: LeNet 5 is initially designed for the input size of 28 by 28. Since Fashion and Digit MNIST already use the same size, we did not change any hidden units of original LeNet 5. For the light CNN, convolutions filter numbers of 3 and 6 are used in the first and second layers. Consequently, hidden unit sizes are: 96, 64 and 42, respectively.

Supplementary Table 1. The accuracy comparison of nPOLO framework with digital convolutional neural networks.

Network Type	Imagenette	Fashion MNIST	Digit MNIST
LeNet 5 (1st Layer: 6 filters, 2nd Layer: 16 filters)	51.06	89.36	98.98
Light CNN (1st Layer: 3 filters, 2nd Layer: 6 filters)	45.7	88.28	98.5
nPOLO	46.3	86.13	96.43

Supplementary Reference

1. LeCun, Y. et al. Backpropagation Applied to Handwritten Zip Code Recognition. *Neural Comput.* 1, 541–551 (1989).